Static and Fatigue Behavior of Short-Headed Studs Embedded in a Thin Ultrahigh-Performance Concrete Layer

Junhui Cao[1]; Xudong Shao, Ph.D.[2]; Lu Deng, Ph.D., M.ASCE[3]; and Yidong Gan[4]

Abstract: In recent years, ultrahigh-performance concrete (UHPC) has been increasingly applied to orthotropic steel deck (OSD) bridges. The UHPC layer and the OSD are connected through short-headed studs. This paper studies the static and fatigue behavior of short-headed studs embedded in UHPC. Seven specimens were fabricated for push-out tests, three of which were subjected to static tests, and the other four were subjected to fatigue tests. The headed studs in these specimens had a low height-to-diameter ratio of 2.7. Both the static and fatigue tests showed that the specimens failed because of the fracture of the headed studs, whereas the UHPC layer did not develop appreciable damage. These observations reflected the fact that the short-headed studs developed full strength when embedded in UHPC. Based on the fatigue test results, a design *S-N* curve with 95% survival probability was proposed. **DOI: 10.1061/(ASCE)BE.1943-5592.0001031.**

Author keywords: Ultrahigh-performance concrete (UHPC); Short-headed stud; Push-out test; Shear stiffness; Relative slip; *S-N* curve.

Introduction

Headed studs are a type of shear connectors commonly used in steel-concrete composite structures. Numerous studies have been performed to investigate the behavior of headed studs under static loads (Ollgaard et al. 1971; Xue et al. 2008), fatigue loads (Hanswille et al. 2007a; Mainston and Menzies 1967), and cyclic loads (Civjan and Singh 2003).

Most relevant studies performed are within the following scopes: (1) the concrete is predominantly normal concrete or lightweight concrete with a compressive strength of ≤ 80 MPa; and (2) the studs usually have a height-to-diameter ratio greater than 4.0, a critical value below which the studs may not develop full strength (Slutter and Driscoll 1961). However, with the development of ultrahigh-performance concrete (UHPC) and its fast-growing applications in steel-concrete composite structures, whether the conclusions from previous studies are still applicable becomes a question.

UHPC is a class of concrete with high strength and excellent durability. Owing to the advantages of high strength and reliable durability, UHPC structures can be much thinner and lighter than conventional concrete structures. For example, Shao et al. (2013) proposed a new composite deck composed of an orthotropic steel deck (OSD) and an UHPC layer, which is also referred to as a lightweight composite deck (LWCD). In the LWCD, the UHPC layer is only 35–60 mm thick, significantly thinner than the thickness of normal concrete decks (200–400 mm) as required for conventional steel-concrete composite bridges.

To guarantee that the UHPC layer works well together with the OSD, an effective interfacial connection is desired. Buitelaar et al. (2004) suggested using epoxy adhesive, whereas Murakoshi et al. (2007) proposed a hybrid method in which the epoxy adhesive connection was supplemented by a subsidiary connection provided by sparsely distributed headed studs. Dieng et al. (2013) used small shear connectors to connect the UHPC layer and the OSD, and this method has been applied to a pilot bridge in France (Hajar et al. 2013). In all of the aforementioned schemes, the concrete layers function as overlays rather than structural components. In these cases, adhesive can provide adequate connection for the cement-based overlays, with a service life much shorter than that of a structure. However, regarding the LWCD, the UHPC layer is a structural component (Shao et al. 2013), which requires that a robust composite action be developed at the interface, and the UHPC layer is expected not to develop appreciable damage during the lifetime of the bridge deck. According to studies by Dieng et al. (2013), the stronger the composite action is, the lower the stresses in both the UHPC layer and the OSD are. In general, adhesive is made of organic compounds that will age with time, and therefore, the service life of the adhesive layers is limited.

Considering all of the aforementioned facts, headed studs are used in the present study. To allow for the shallow depth of the UHPC layer, small-headed studs with a typical height-to-diameter ratio of h/d = 35/13 mm = 2.7 are preferred. Headed studs, which are welded to steel plates through drawn-arc automatic welding, are actually commonly used in practice, and the cost involved in welding construction is acceptable.

There have been studies on the shear connectors embedded in UHPC. Kim et al. (2015) performed static push-out tests on headed studs embedded in UHPC. The tests showed that the aspect ratio of the headed studs can be reduced from a common value of 4.0 to 3.1 without reducing the shear strength of the studs. Luo et al. (2015a) investigated the static behavior of headed studs in a steel-fiber-reinforced cementitious composite (SFRCC) with a compressive strength of 120–150 MPa, and it was found that a SFRCC slab without any rebar still ensures a failure mode of stud fracture. In addition, Kang et al. (2014) and Rauscher and Hegger (2008)

[1]Ph.D. Candidate, Key Laboratory for Wind and Bridge Engineering of Hunan Province, Hunan Univ., Changsha 410082, China. E-mail: caojunhui@hnu.edu.cn

[2]Professor, Key Laboratory for Wind and Bridge Engineering of Hunan Province, Hunan Univ., Changsha 410082, China (corresponding author). E-mail: shaoxd@hnu.edu.cn

[3]Professor, Key Laboratory for Wind and Bridge Engineering of Hunan Province, Hunan Univ., Changsha 410082, China. E-mail: denglu@hnu.edu.cn

[4]Graduate Student, Key Laboratory for Wind and Bridge Engineering of Hunan Province, Hunan Univ., Changsha 410082, China. E-mail: ganyd_123@163.com

Note. This manuscript was submitted on July 6, 2016; approved on November 18, 2016; published online on February 9, 2017. Discussion period open until July 9, 2017; separate discussions must be submitted for individual papers. This paper is part of the ***Journal of Bridge Engineering***, © ASCE, ISSN 1084-0702.

investigated the static behaviors of continuous shear connectors in UHPC; Li et al. (2016) reported fatigue test results on 35-mm short-headed studs in UHPC.

However, in all of the aforementioned tests, the thickness of the UHPC layers is predominantly 75–150 mm, significantly exceeding that of the UHPC layer in the LWCD. Furthermore, most of these studies highlight the static behavior of the shear connectors, and few studies are available regarding the fatigue performance. Thus, it is necessary to perform static and fatigue tests for the short-headed studs in the thin UHPC layer used in the LWCD.

In this paper, seven push-out specimens were fabricated, three of which were subjected to static tests, and the other four were subjected to fatigue tests. Based on the test results, the behaviors of short-headed studs embedded in UHPC were revealed: the failure mode was revealed, the load-slip relationships were obtained, and an *S-N* curve was developed.

Static Load Tests

Test Setup and Specimen Dimensions

The behavior of headed studs against shear loads can be revealed through tests on either push-out specimens or steel-concrete composite beam specimens. With advantages such as small specimen sizes and low stress redistribution in the headed studs, push-out specimens have been widely used since first attempted in Switzerland in the 1930s. In this study, push-out specimens were adopted in both static and fatigue tests.

Seven push-out specimens with identical configurations were fabricated (Fig. 1). Each specimen consisted of an I-shaped steel part and two 50-mm UHPC flanges, as shown in Fig. 1. Each UHPC flange was connected to the steel plate via four short-headed studs. With a diameter of 13 mm and a height of 35 mm, the headed studs have a low height-to-diameter ratio of 2.7 and have a cover thickness of 15 mm. The UHPC layer was reinforced by the HRB400 steel rebar, a type of ribbed steel rebar commonly used in China with a nominal yield strength of 400 MPa. The steel rebar had a diameter of 8 mm and was deployed with central spacings of 50 and 65 mm along the loading and transversal directions, respectively. A 15-mm-thick cover was used for the steel bars.

The UHPC used in this paper was specially developed for the LWCDs by the research group at Hunan University, Hunan Sheng, China. A detailed list of the ingredients in UHPC can be found in Table 1. The maximum grain size of the quartz sand used in UHPC is 0.9 mm. The UHPC layers were steam cured for a period of 48 h under a temperature ranging from 103 to 108°C in this study. Generally, the curing temperature for UHPC should be no lower than 90°C.

The three specimens subjected to static loads were named STA-1, STA-2, and STA-3, respectively. The tests were conducted with a 2,000-kN compression testing machine (Fig. 2). The specimens were placed on a fixed steel platform, and the load was exerted through a loading plate on the top. A force transducer was installed between the loading plate and the support to control the load precisely.

Considering that each specimen contains eight headed studs, eight dial indicators were installed on the sides of each specimen to record the relative slips at the interface between the steel and UHPC. Prior to the test, preloading was applied with a load of

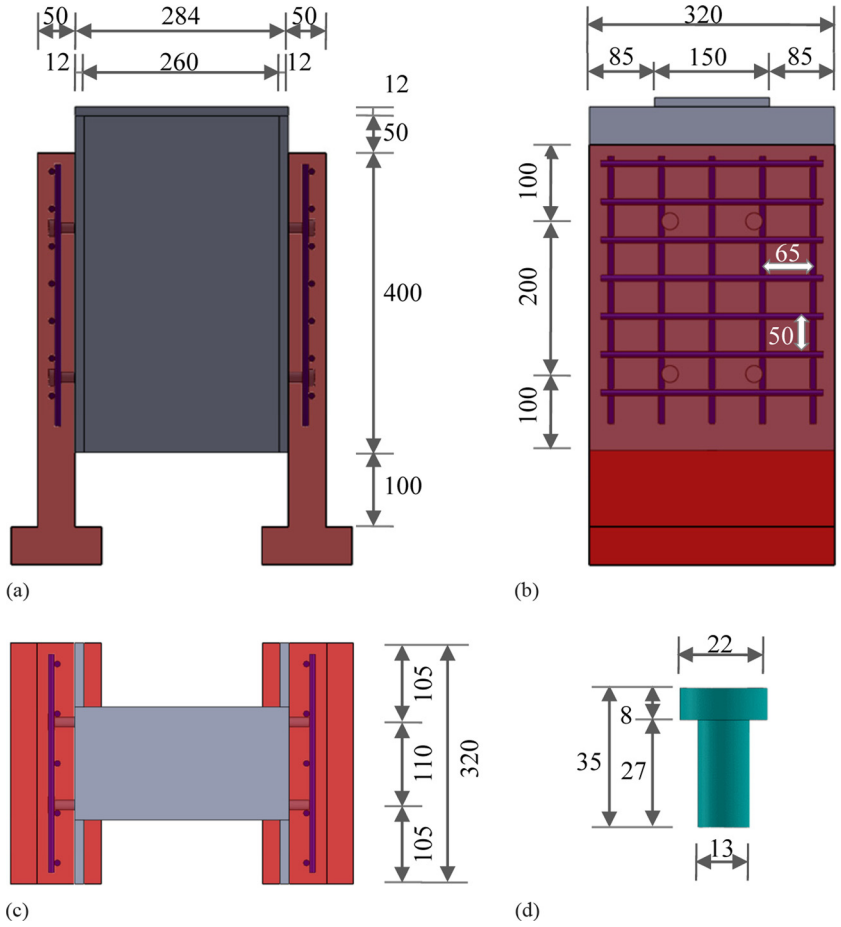

Fig. 1. Push-out specimens (units: mm): (a) front view; (b) side view; (c) top view; (d) dimensions of headed stud

100 kN to ensure that both the loading system and the dial indicators work well. During the test, the load was increased monotonically by an increment of 25 kN at each step until failure occurred in the specimens. Within each load-increasing step, the loading rate was controlled at 0.08 kN/s. After each load increment was completed, a time gap of 5 min was reserved to stabilize the load and to record the slips at the steel–UHPC interfaces.

Test Results

The three specimens had a similar failure mode: the studs on either side of the specimens (i.e., Side A or Side B) were sheared off from the steel plate, resulting in a complete separation between the UHPC layer and the remaining part of the specimen. Fig. 3 shows the typical failure mode. It can be seen that the headed studs were sheared off from the steel plate and were still embedded in UHPC.

The inner interfaces on both the steel plate and the UHPC layer were carefully scrutinized. Two fracture positions were observed on the headed studs. In the first case, the fracture surface was a small concave on the steel plate, below the stud-to-steel-plate weld [Fig. 4(a)], whereas in the second case, the fracture surface was in the stud shank, above the stud-to-steel-plate weld [Fig. 4(b)].

It was also observed that the UHPC layer was intact on the outside, with no cracking, crushing, or splitting observed. On the inner side, only very limited damage was developed within a small region around the headed studs. In Fracture Position 1, the UHPC was crushed in front of the stud and was cracked behind the stud, whereas in Fracture Position 2, the UHPC was spalled around the stud.

Tests on the three specimens revealed that they had shear strengths of 487.8, 457.1, and 497.5 kN, respectively. Because each specimen has eight headed studs, the average shear strength per stud was obtained as 61.0, 57.1, and 62.2 kN, respectively.

Table 1. Ingredients of UHPC

Item	Ingredients	Value
Weight (kg/m^3)	Cement	771.2
	Silica fume	154.2
	Fly ash	77.1
	Quartz sand	848.4
	Quartz powder	154.2
	Superplasticizer	20.1
	Water	180.5
	Steel fibers	
	Type 1	118
	Type 2	157
Weight ratio	Cement	1.0
	Silica fume	0.2
	Fly ash	0.1
	Quartz sand	1.1
	Quartz powder	0.2
	S/P ratio (%)	2
	W/P ratio	0.18
Volume ratio (%)	Type 1 fraction	1.5
	Type 2 fraction	2.0

Note: For superplasticizer, *S/P ratio* means the weight ratio of superplasticizer to paste material (including cement, silica fume, and fly ash); for water, *W/P ratio* means the weight ratio of water to paste material (including cement, silica fume, and fly ash); for steel fibers, Type 1 denotes steel fibers with $D = 0.12$ mm and $L = 8$ mm, and Type 2 denotes steel fibers with $D = 0.2$ mm and $L = 13$ mm, where D denotes fiber diameter, and L denotes fiber length.

Result Analysis and Discussion

Shear Strength and Failure Mode

Because no equations for predicting the shear strength of headed studs in UHPC are available, the equations in normal concrete are presented here to discuss the failure mode and the shear strength.

For headed studs in normal concrete, there are two failure modes (i.e., crush of concrete plate and fracture of headed studs). The failure modes are influenced by different parameters. According to the AASHTO LRFD (AASHTO 2012) specifications, the shear strength of headed studs can be calculated by Eq. (1). The left part of the equation corresponds to the concrete failure mode, and the right part corresponds to the stud failure mode

$$Q_u = \phi 0.5 A_{sc} \sqrt{f_c' E_c} \le \phi A_{sc} f \tag{1}$$

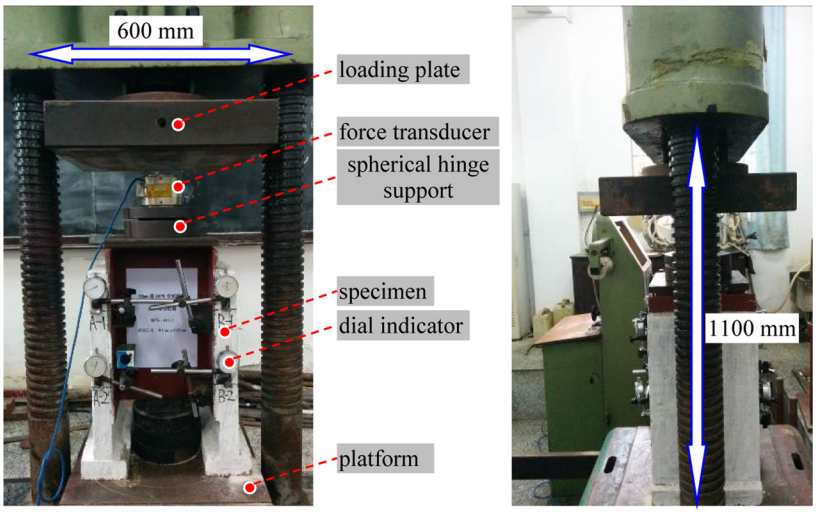

Fig. 2. Static test setup: (a) front view; (b) side view

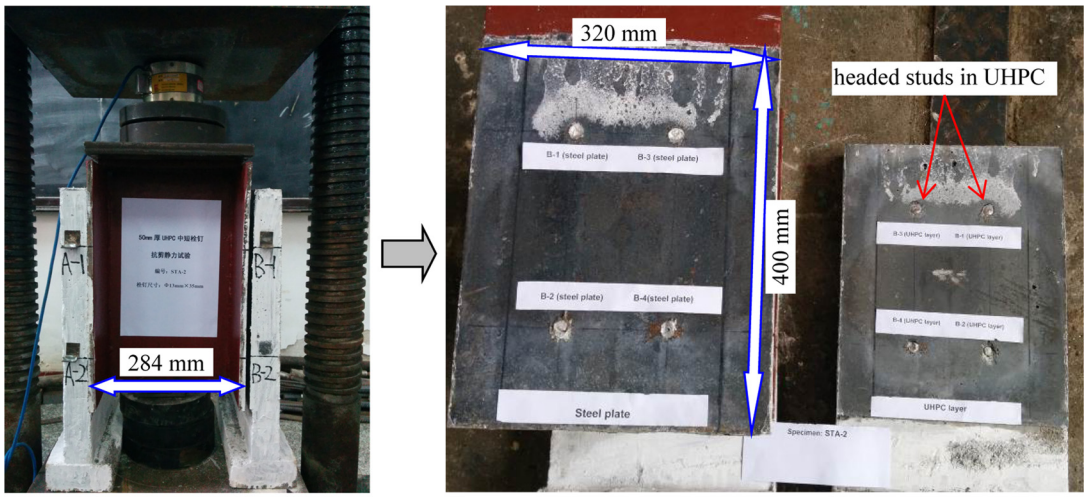

(a) (b)

Fig. 3. Failure mode of specimen in the static tests: (a) front view of the specimen; (b) two separated parts

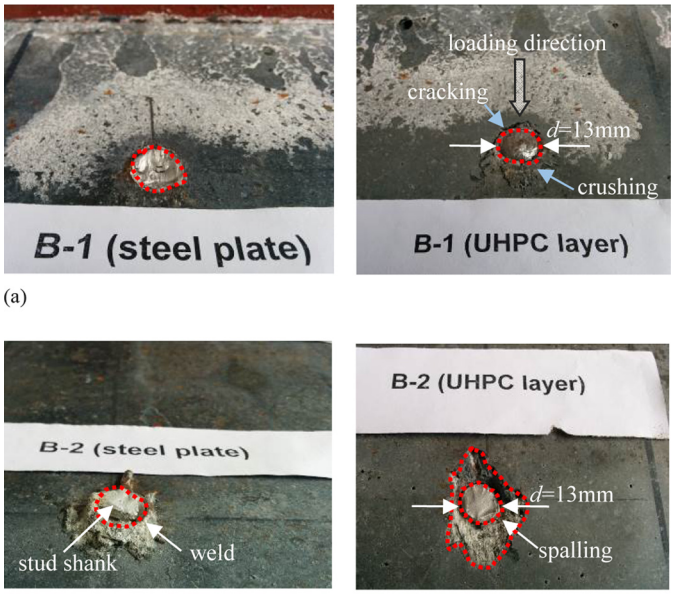

(a)

(b)

Fig. 4. Two fracture positions of headed studs: (a) Failure Position 1 (from weld); (b) Failure Position 2 (from stud shank)

where A_{sc} = sectional area of headed studs (mm^2); f_c' = compressive strength of concrete cylinders (MPa); E_c = modulus of elasticity of concrete (MPa); f = tensile strength of headed studs (MPa); and ϕ = resistance reduction factor, whose value is 0.85.

The Chinese *Code for design of steel and concrete composite bridges* (MHURDOC 2013) also provides a formula to calculate the shear strength of headed studs, as shown in Eq. (2)

$$Q_u = 0.43\,\eta A_{sc}\sqrt{f_{cd}E_c} \le 1.19A_{sc}f\left(\frac{E_c}{E_s}\right)^{0.2}\left(\frac{f_{cu}}{f}\right)^{0.1} \tag{2}$$

where A_{sc} = sectional area of headed studs (mm^2); f_{cd} and f_{cu} = design compressive strength of concrete prisms and compressive strength of concrete cubes, respectively (MPa); E_c and E_s = modulus of elasticity of concrete and headed studs, respectively (MPa); f = tensile strength of headed studs (MPa); and η = reduction factor due to the group stud effect, which is taken as 1.0 when $l_d/d \ge 13$ (l_d and d denote the longitudinal spacing and the diameter of headed studs, respectively).

The equation in Eurocode 4 (ECS 2005) is shown in Eq. (3). The height-to-diameter ratio is taken into account when considering the concrete failure mode on the left part of the equation

$$Q_u = 0.29\alpha d^2\sqrt{f_c'E_c}/\gamma_v \le 0.8A_{sc}f/\gamma_v \tag{3}$$

where α = factor considering the height-to-diameter ratio, whose value is $\alpha = 0.2(h/d+1) \le 1.0$ when $h/d \ge 3$, in which h and d are the height and diameter of headed studs, respectively; f_c' = compressive strength of concrete cylinders (MPa); E_c = modulus of elasticity of concrete (MPa); A_{sc} = sectional area of headed studs (mm^2); f = tensile strength of headed studs; and γ_v = material partial factor, whose value is 1.25.

According to Eqs. (1)–(3), there exists a critical compressive strength of concrete, beyond which the failure mode will always be the fracture of headed studs. Shariati et al. (2012) stated that the critical compressive strength was f_c' = 30–37 MPa. Thus, it is not surprising that all three of the specimens in this paper failed due to the fracture of the headed studs because the UHPC used in this study has a compressive strength of 130–155 MPa (Shao et al. 2013), significantly higher than the critical compressive strength of concrete.

The aforementioned equations are all for headed studs embedded in normal concrete. According to relevant studies (An and Cederwall 1996; Hegger et al. 2001), when headed studs are imbedded in high-strength concrete, their mechanical behaviors differ significantly from those embedded in normal concrete. The presence of a weld collar also affects the strength of the headed stud. Based on the results from push-out tests, Doinghaus et al. (2003) proposed a formula specifically for the shear strength of headed studs imbedded in high-strength concrete with a compressive strength of no less than 55 MPa [Eq. (4)], in which the influence of the weld collars is included. In this formula, only one failure mode (i.e., stud failure) is considered

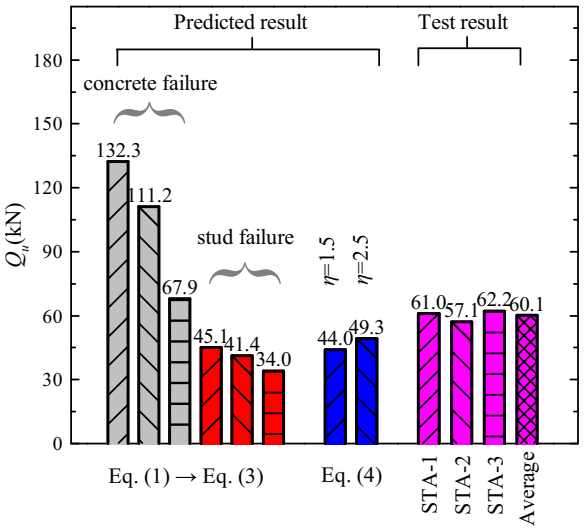

Fig. 5. Comparison between predicted shear strength and tested shear strength

$$Q_u = (0.85A_{sc}f + \eta f_c' d_{wc} l_{wc})/\gamma_v \quad (4)$$

where A_{sc} = sectional area of the headed stud (mm^2); f = tensile strength of the headed stud (MPa); η = coefficient of shear strength improvement caused by the weld collar; f_c' = compressive strength of concrete cylinders (MPa); d_{wc} = diameter of the weld collar (mm); l_{wc} = height of the weld collar (mm); and γ_v = material partial factor, whose value is 1.25.

For headed studs in high-strength concrete, although a consensus was reached that the weld collar contributes to the shear strength, the value of η is different according to different references. In the formula proposed by Doinghaus et al. (2003), the value of η is 1.5 for conventional high-strength concrete. However, Luo et al. (2015b) stated that the value is not enough for concrete with higher compressive strength. Based on push-out tests, they stated that a value of $\eta = 2.5$ is more suitable for steel-fiber-reinforced concrete with a compressive strength up to 120–150 MPa.

To compare the predicted shear strength of headed studs to that calculated based on push-out test results, calculations were performed based on Eqs. (1)–(4), and the results are shown in Fig. 5. When using Eq. (4), the sizes of the weld collar should be provided. For the headed studs in this paper, the weld collar had a nominal diameter of d_{wc} = 17 mm and a height of l_{wc} = 3 mm (GAQSIQOC 2002). Two weld collar–related factor values (i.e., η = 1.5 and 2.5) were examined. The UHPC had a compressive strength of f_{cu} = 135.9 MPa and a modulus of elasticity of E_c = 42.6 GPa (Shao et al. 2013). In addition, experimental tests by Graybeal (2005) indicated that the compressive strength of UHPC derived from cylinders and cubes did not exhibit significant differences. Thus, the compressive strength of UHPC cylinders could be obtained as $f_c' = 0.95\ f_{cu}$ = 129.1 MPa (Graybeal 2005). Headed studs have a tensile strength of f = 400 MPa (MHURDOC 2013).

Fig. 5 clearly shows that, for Eqs. (1)–(3), the predicted shear strengths based on the concrete failure mode are much higher than those based on the stud failure mode, indicating that the failure mode should be stud failure. Furthermore, the predicted shear strengths by using the right part of Eqs. (1)–(3) are approximately 25–43% lower than the real shear strength obtained from the tests (Q_u = 60.1 kN on average). Thus, Eqs. (1)–(3) can significantly underestimate the shear strength of the headed studs embedded in UHPC. This will lead to a conservative design.

The calculation results based on Eq. (4) show a better agreement with the test results. With the weld collar–related coefficient taken as η = 1.5 and 2.5, the predicted shear strengths are 27 and 18% lower than the average tested result, respectively. Thus, for headed studs in UHPC, the weld collar contributes to a significant portion of the shear strength and should be taken into account in the strength prediction. In addition, $\eta = 2.5$ leads to an even closer result relative to the test results.

Load-Slip Curve

The load-slip curves are plotted in Fig. 6. Under each load level of the subfigures, Side A and Side B denote the average slips observed from the four dial indicators on each side [i.e., $s_A = (1/4)\sum_1^4 s_{i,A}$ and $s_B = (1/4)\sum_1^4 s_{i,B}$], whereas *average of A and B* denotes the average slip of the two sides [i.e., $s = (s_A + s_B)/2$. It is clear from Figs. 6(a–c) that, although the slips on the two sides were not identical, both slips increased smoothly with the increasing load.

Fig. 6(d) shows that the averaged load-slip curves of the three specimens are quite close to each other. It can also be seen from the figure that the headed studs as a group began to yield at a load of approximately 400 kN, beyond which the slips increased significantly with a small increase of the load.

Shear Stiffness

Shear stiffness is an important parameter in the design of composite structures. A number of methods are available for the calculation of shear stiffness for headed studs. Wang (1998) proposed that the design shear strength of a stud should be 0.8 times its actual shear strength, and the corresponding slip was 0.8 mm. As a result, the shear stiffness of a stud can be calculated as $k = Q_u$ (kN/mm), where Q_u is the shear strength of a stud. Nie and Shen (1994) proposed a concise equation after performing statistical analysis on a large number of experimental data [i.e., $k = 0.66\ Q_u$ (kN/mm)]. However, these methods predicted the shear stiffness by utilizing empirical coefficients that were derived from the database of headed studs embedded in normal concrete. Thus, these methods were not used in the present study.

In another method, the shear stiffness of headed studs is calculated based on the load-slip curve. The shear stiffness is defined as the slope of a secant line on the load-slip curve. The lower point of the secant line is the original point, and the upper point is different according to different methods. Johnson and May (1975) defined the upper point as the half shear strength point, JSSC (2002) prefers to use the one-third shear strength point, and Eurocode 4 (ECS 2005) specifies that the upper point should be 0.7 times the shear strength. Considering that the secant slope method captures the shear stiffness based on the load-slip curve rather than merely based on the shear capacity, the shear stiffness obtained by this method is not affected by the type of shear connectors (e.g., rigid or ductile) and the compressive strength of concrete (e.g., normal concrete, high-strength concrete, or UHPC). Therefore, the secant slope method was adopted in the present study. It should be noted that the shear stiffness (k) listed in Table 2 is for a single-headed stud.

According to Table 2, the calculated shear stiffness of headed studs is influenced by the method adopted. The higher the upper point of the secant line is, the lower the shear stiffness is. The shear stiffness of the headed studs obtained from the three methods varied between 266 and 396 kN/mm for one stud.

To compare the shear stiffness of the headed studs in UHPC to that of headed studs in normal concrete, a load-slip curve equation proposed by Ollgaard et al. (1971) for headed studs in normal concrete is used to calculate the slips under different load levels [Eq. (5)]

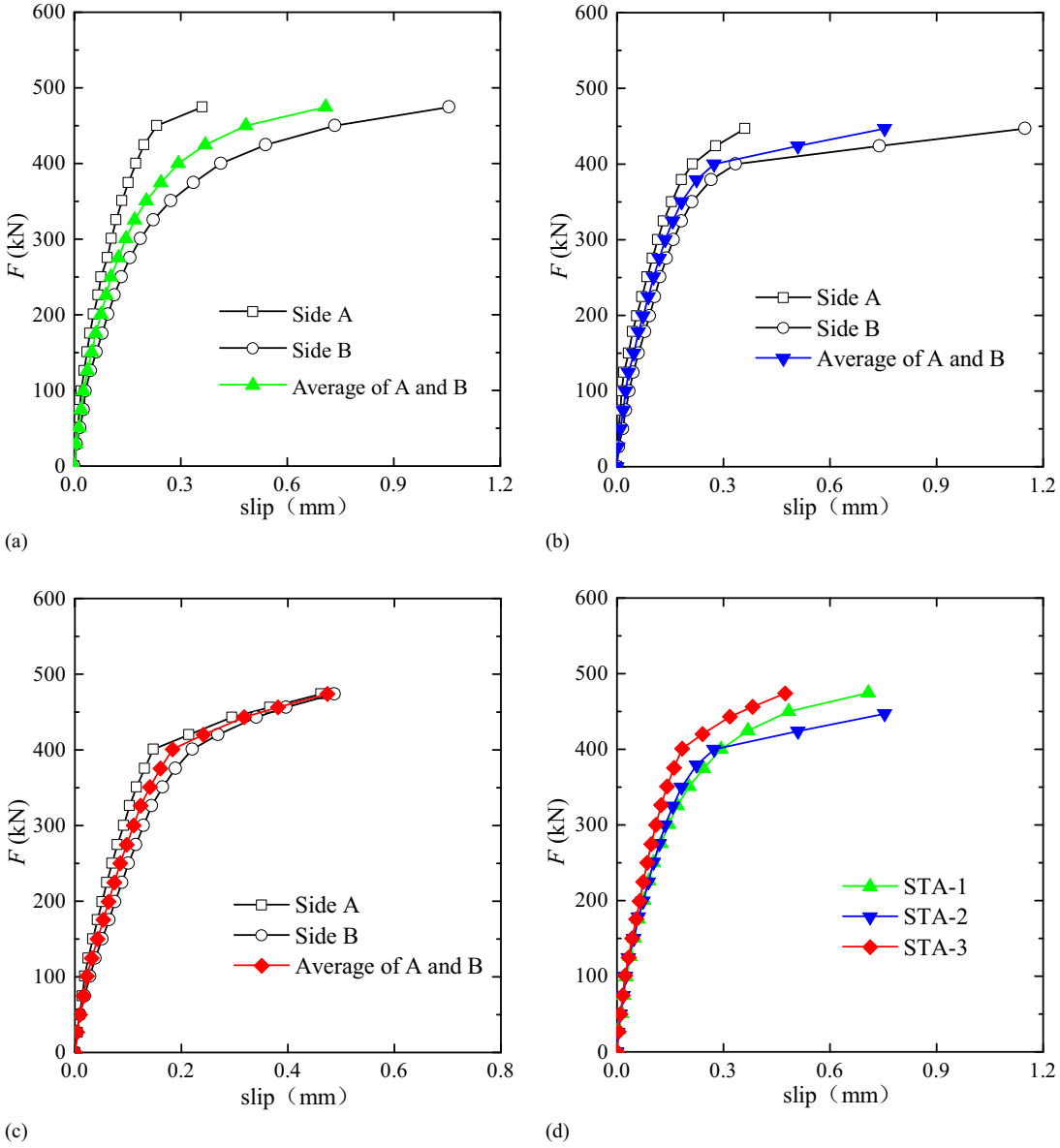

Fig. 6. Load-slip curves in static tests: (a) Specimen STA-1; (b) Specimen STA-2; (c) Specimen STA-3; (d) collection of all three specimens

Table 2. Shear Stiffness Calculation

Reference	Parameters	Specimen			Average of k	Unit
		STA-1	STA-2	STA-3		
JSSC (2002)	$1/3Q_u$	162.6	152.4	165.8	—	kN
	Slip at $1/3Q_u$	0.0549	0.0479	0.0492	—	mm
	k per stud	369.9	397.8	421.6	396.4	kN/mm
Johnson and May (1975)	$0.5Q_u$	243.9	228.6	248.8	—	kN
	Slip at $0.5Q_u$	0.1005	0.0902	0.0848	—	mm
	k per stud	303.3	316.9	366.6	328.9	kN/mm
Eurocode 4 (ECS 2005)	$0.7Q_u$	341.5	320.0	348.3	—	kN
	Slip at $0.7Q_u$	0.1916	0.1529	0.1387	—	mm
	k per stud	222.8	261.7	313.9	266.1	kN/mm

$$F/Q_u = (1 - e^{-18s})^{0.4} \quad (5)$$

where F = shear load (kips); Q_u = shear strength per headed stud (kips); and s = interfacial slip (in.).

Assuming that a headed stud (with a diameter of 13 mm) embedded in normal concrete has a shear strength identical to the headed studs investigated in this paper (i.e., Q_u = 60.1 kN), according to Eq. (5), the slips under different load levels of

F/Q_u = 0.33, 0.5, and 0.7 were calculated to be 0.094, 0.275, and 0.744 mm, respectively. By following the same calculating procedures as presented in Table 2, the shear stiffness of the headed stud embedded in normal concrete can be determined, and the results are listed in Table 3.

As can be seen in Table 3, the shear stiffness of the headed studs in UHPC is much higher than that in normal concrete. The closer the reference load level is to the ultimate shear strength, the higher the difference of the shear stiffness is. The observation is similar to that reported by Kim et al. (2015). According to their study, a stud embedded in the UHPC provides at least 60% higher stiffness than that in normal concrete. Therefore, a higher shear stiffness implies higher efficiency in developing a composite action, which is beneficial to the composite action between the thin UHPC layer and the OSD.

Fatigue Load Tests

Test Setup and Loading Programs

To reveal the behavior of headed studs against fatigue loads, four push-out specimens (i.e., FAT-1, FAT-2, FAT-3, and FAT-4) were subjected to fatigue loads. The configuration of the push-out specimens is shown in Fig. 1, and the test setup is shown in Fig. 7.

During the tests, the specimens were fixed to the ground through bolt-anchored steel plates. The fatigue tests were conducted through a hydraulic impulse fatigue-testing machine. The fatigue load was applied from the top of the specimen by a 250-kN actuator.

Table 3. Comparison of Shear Stiffness for Headed Studs in Different Concrete

Reference	Reference load level	In normal concrete (kN/mm)	In UHPC (kN/mm)	Stiffness increment (%)
JSSC (2002)	$1/3Q_u$	214.13	396.4	85
Johnson and May (1975)	$0.5Q_u$	109.47	328.9	200
Eurocode 4 (ECS 2005)	$0.7Q_u$	56.51	266.1	371

In the fatigue tests, apart from the real-time dynamic slip that was monitored throughout the fatigue test, the static slip was also recorded. When the loading cycles reached certain values, the fatigue loading was suspended for a while, and a static load test was performed instead to obtain the slip. The two types of slip were recorded through different apparatuses: the dynamic slip was recorded via a portable QuantumX dynamic data collector and two WA-100 dynamic displacement sensors (Hottinger Baldwin Messtechnik, Darmstadt, Germany), and the static slip was recorded via mechanical dial indicators, as shown in Fig. 8. The dynamic slip was recorded with a sampling frequency of 100 Hz. To guarantee that the relative slips between the steel plates and the UHPC layers were recorded, small segments of angle steel were glued to the side of the UHPC layer, to which the tips of the sensors and indicators were touched.

In a fatigue test, the fatigue stress can be represented by three parameters [i.e., maximum stress (σ_{max}), minimum stress (σ_{min}), and load frequency (f)] as shown in Fig. 9. Generally speaking, the fatigue life of a steel component is governed by both the maximum and minimum stresses, and the two parameters are more commonly expressed in another form: stress range ($\Delta\sigma = \sigma_{max} - \sigma_{min}$) and stress ratio ($R = \sigma_{min}/\sigma_{max}$). However, for as-welded steel connections, high residual stresses close to the yield strength of steel may exist. When the steel connection is exposed to external loads, the load-induced stress is superimposed to the residual stress. Thus, even when the load-induced stress is low, the actual stress in the steel components around the welds may be very high. In this case, the fatigue life is mainly governed by the stress range ($\Delta\sigma$). As a result, the *S-N* curves used in fatigue design of welded steel connections commonly have stress range as an independent variable.

The aforementioned principle is also applicable to steel-concrete composite structures with headed studs welded to steel plates. According to fatigue tests by Slutter and Fisher (1966), the most important factor that influences the fatigue life of headed studs is the shear stress range. Thus, for the fatigue tests in this paper, the four specimens were loaded with different shear stress ranges (Table 4). During the tests, all of the specimens had an equal stress ratio (R), and the reason was that the International Institute of Welding (IIW) (Hobbacher 2007) recommends that, when fatigue tests are used to establish an *S-N* curve for fatigue-prone details, the stress ratio should be maintained at a constant level. In Table 4, F denotes the

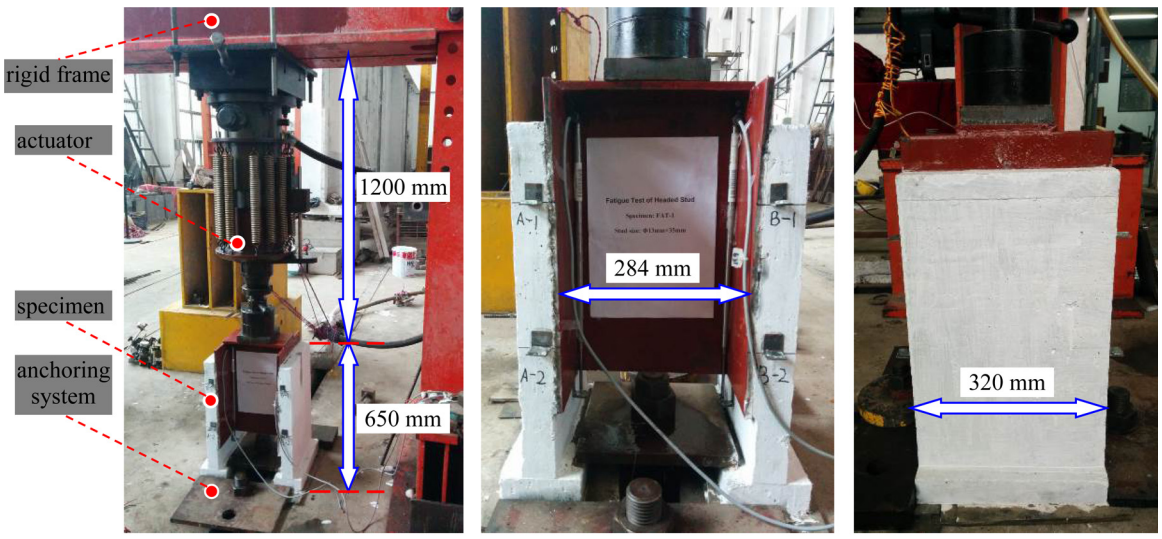

Fig. 7. Fatigue test setup: (a) overall view; (b) front view; (c) side view

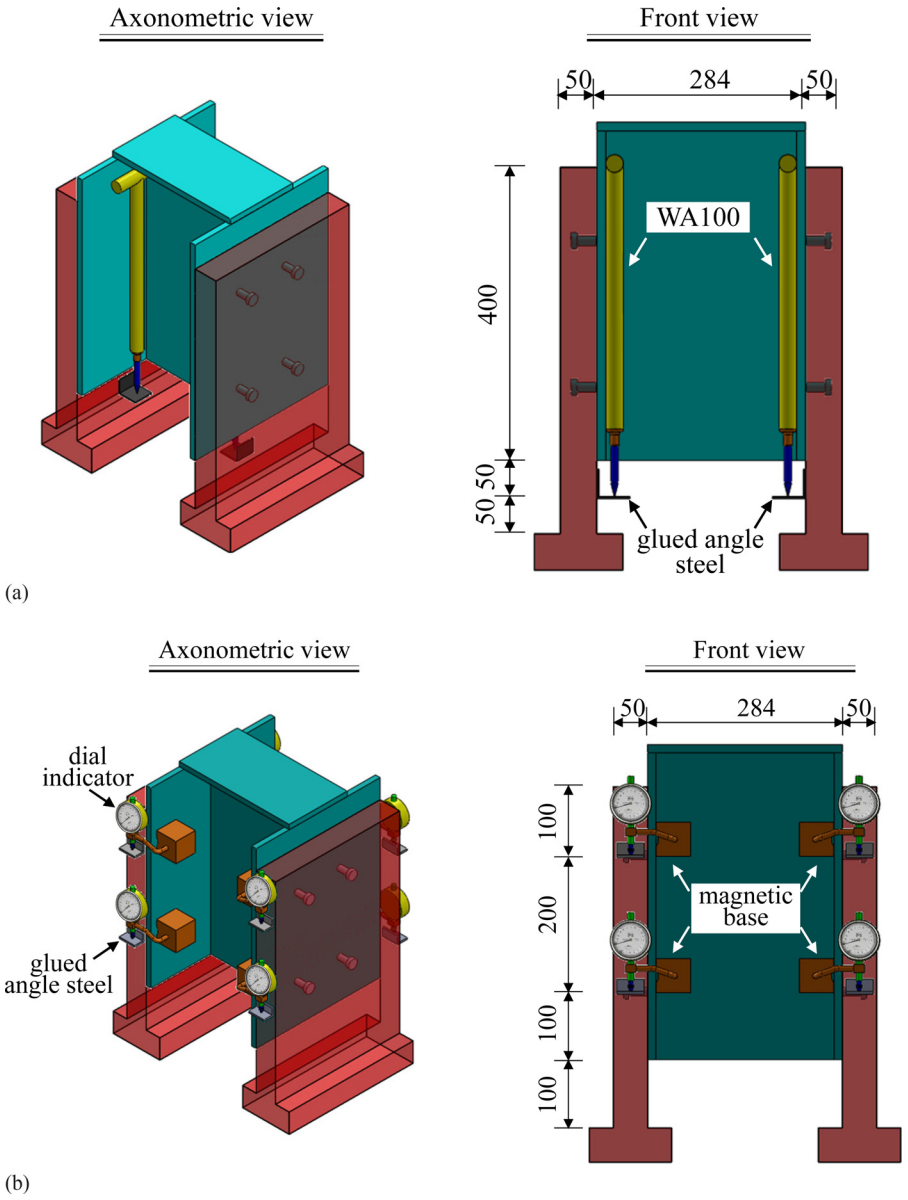

Fig. 8. Slip-recording apparatus (units: mm): (a) dynamic slip; (b) static slip

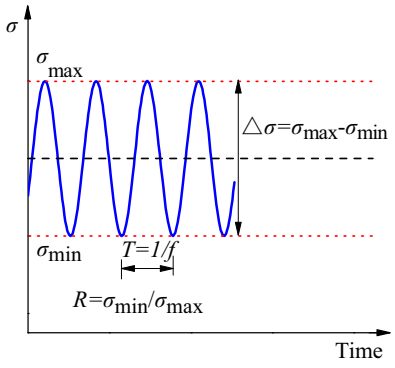

Fig. 9. Key parameters in cyclic fatigue loading

load applied to a specimen, and τ denotes the nominal shear stress per headed stud and is calculated as $\tau = (F/8)/A_{sc}$, where A_{sc} is the sectional area of a headed stud.

Considering that the fatigue tests in this paper were intended to establish an *S-N* curve for the headed studs in UHPC, all specimens were tested until failure occurred. Thus, no run-out cycles were defined for the present fatigue tests.

Test Results

The four specimens revealed a similar failure mode. The headed studs on one side of the specimens (i.e., either Side A or Side B) were sheared off from the steel plate, leading to a complete separation between the UHPC layer and the remaining part of the specimen, whereas the opposite side of the specimen was still in good status, with no separation. The observed failure mode is shown in Fig. 10.

Similar to the two fracture positions observed in the static tests, there were also two fracture positions for the headed studs in the fatigue tests. In the first fracture position, fatigue cracks initiated from the weld toe and propagated downward into the steel plate. In the second fracture position, fatigue cracks initiated and propagated in

Table 4. Main Parameters in Fatigue Test

Specimen	Load (kN)			Frequency (Hz)	Nominal shear stress per stud (MPa)			Stress ratio R (τ_{min}/τ_{max})
	F_{max}	F_{min}	ΔF		τ_{max}	τ_{min}	$\Delta\tau$	
FAT-1	122	22	100	5.0–5.5	115	21	94	0.18
FAT-2	151	27	124	5.0	143	26	117	0.18
FAT-3	162	29	133	5.0	152	27	125	0.18
FAT-4	175	31	143	5.0	165	30	135	0.18

Fig. 10. Failure mode of fatigue specimen

the stud shank. The two fracture positions are shown in Fig. 11. The main test results are listed in Table 5.

Results Analysis and Discussion

S-N Curve of Headed Studs Embedded in UHPC

The *S-N* curve, also called the Wöhler curve, is a fundamental tool for fatigue design of steel structures. The *S-N* curve reveals the relationship between the fatigue life and stress range, as shown in Eq. (6)

$$m \log \Delta\tau + \log N = C \tag{6}$$

where m = slope of the *S-N* curve; $\Delta\tau$ = stress range in the fatigue-prone detail; N = fatigue life of the detail; and C = fatigue constant.

Several standards have provided *S-N* curves for headed studs embedded in normal concrete. For example, in Eurocode 4 (ECS 2005), the *S-N* curve of headed studs has a slope of $m = 8$ and a fatigue strength of 90 MPa at 2 million cycles. However, regarding headed studs embedded in UHPC, there are still no relevant *S-N* curves available.

In this study, results from four fatigue test specimens were obtained. In an early study by the authors, a similar fatigue test was undertaken on some other push-out specimens of the same kind under the same testing conditions (Li et al. 2016). Therefore, the fatigue test results obtained from that study could also be used in the data analysis. However, of the specimens reported in the other study (Li et al. 2016), only one was tested to failure. The failed specimen failed after $N_f = 620{,}000$ cycles under a shear stress range of $\Delta\tau = 145$ MPa.

By performing curve-fitting using the five fatigue data points in a log–log coordinate system, a linear relationship could be found between $\Delta\tau$ and N_f, as shown in Fig. 12. The fitted line had a slope of $m = 8.2713$, which is close to that for headed studs in normal concrete (i.e., $m = 8$), indicating that, although the number of specimens in this paper is relatively small, the test results could still reasonably reflect the fatigue characteristics of the headed studs in UHPC against fatigue loads. According to the IIW (Hobbacher 2007), the slope can be obtained either by linear fitting based on the original fatigue data or by taking a given value based on existing *S-N* curves of fatigue-prone details that have similar behavior. The linear fitting results indicate that the headed studs embedded in the UHPC had fatigue behavior similar to the headed studs embedded in normal concrete. Therefore, for the purpose of consistency and convenience, the slope was assumed to have a value of $m = 8$.

With the value of m determined, the next step is to determine the value of C in Eq. (6). According to the IIW (Hobbacher 2007), the line of best fit only has a survival probability of 50%, which is not sufficient to guarantee a sound fatigue design, which usually demands a survival probability of 95%. Thus, the design *S-N* curve should be modified from the line of best fit, which can be realized by calculating the characteristic value of log$C$ (i.e., logC_k). First, the mean and standard variance of log$C$ are calculated by using Eqs. (7) and (8), respectively. Then, logC_k is calculated by Eq. (9)

$$\mu_{\log C} = \frac{\sum \log C_i}{n} \tag{7}$$

$$\sigma_{\log C} = \sqrt{\frac{\sum \left(\mu_{\log C} - \log C_i\right)^2}{n-1}} \tag{8}$$

$$\log C_k = \mu_{\log C} - k\sigma_{\log C} \tag{9}$$

where $\mu_{\log C}$ and $\sigma_{\log C}$ = mean and standard deviation of log$C$, respectively; i = ith fatigue data; n = sample size of the fatigue data; log C_k = characteristic value of log$C$; and k = modification factor, which is related to the sample size and the target survival probability.

Substituting the fatigue test results into Eqs. (7) and (8), it can be determined that $\mu_{\log C} = 22.8456$ and $\sigma_{\log C} = 0.2046$. The standard deviation ($\sigma_{\log C}$) is only 0.9% of the mean value ($\mu_{\log C}$), indicating that, although the sample size of the fatigue data is limited, the scatter of the test results is small. Prior to developing the *S-N* curve, a value should be specified for the modification factor to allow for the survival probability. According to the IIW, the modification factor is related to the number of specimens. Larger modification factors are required for smaller numbers of specimens. For the fatigue

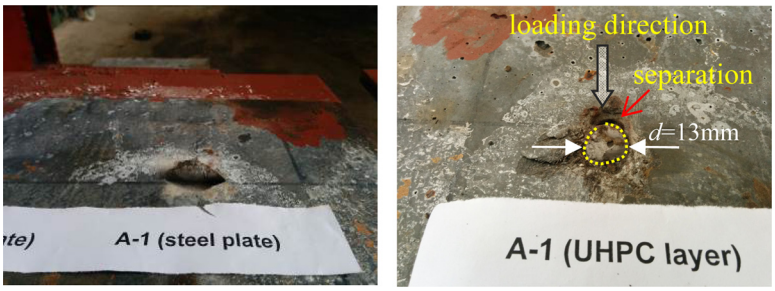

(a)

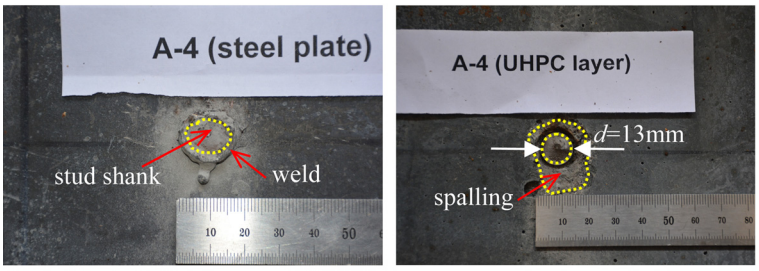

(b)

Fig. 11. Two fatigue fracture positions in headed studs: (a) Fracture Position 1 (weld); (b) Fracture Position 2 (stud shank)

Table 5. Fatigue Test Results

Specimen	Shear stress range per stud [$\Delta\tau$ (MPa)]	Fatigue life [N_f (cycles)]
FAT-1	94	11,787,000
FAT-2	117	1,130,000
FAT-3	125	1,688,000
FAT-4	135	441,000

tests in this paper, the sample size was $n = 5$, resulting in a modification factor of $k = 3.6$. By adopting the modification factor, the influence of the small number of fatigue data on the *S-N* curve was taken into account.

By substituting these values into Eq. (9), the characteristic value of log$C$ is calculated as logC_k = 22.1131. Thus, the *S-N* curves with survival probabilities of 50 and 95% (i.e., the design *S-N* curve) are presented in Eqs. (10*a*) and (10*b*), respectively. For comparison, the design *S-N* curve for headed studs in normal concrete, as specified by Eurocode 4, is presented in Eq. (10*c*). The three curves as well as the five fatigue test data are all plotted in Fig. 12

$$8\log\Delta\tau + \log N = 22.8456 \quad (10a)$$

$$8\log\Delta\tau + \log N = 22.1131 \quad (10b)$$

$$8\log\Delta\tau + \log N = 21.9350 \quad (10c)$$

Fig. 12 shows that all fatigue test data are above the *S-N* curve defined in Eurocode 4. The proposed design *S-N* curve for short-headed studs embedded in UHPC, with a survival probability of 95%, also lies above the *S-N* curve of headed studs embedded in normal concrete. Corresponding to an expected fatigue life of 2 million cycles, the headed studs in normal concrete should have a design fatigue strength of 90 MPa, whereas the headed studs in UHPC should have a fatigue strength of 94.6 MPa. These observations imply that the headed studs have a slightly better fatigue performance in UHPC

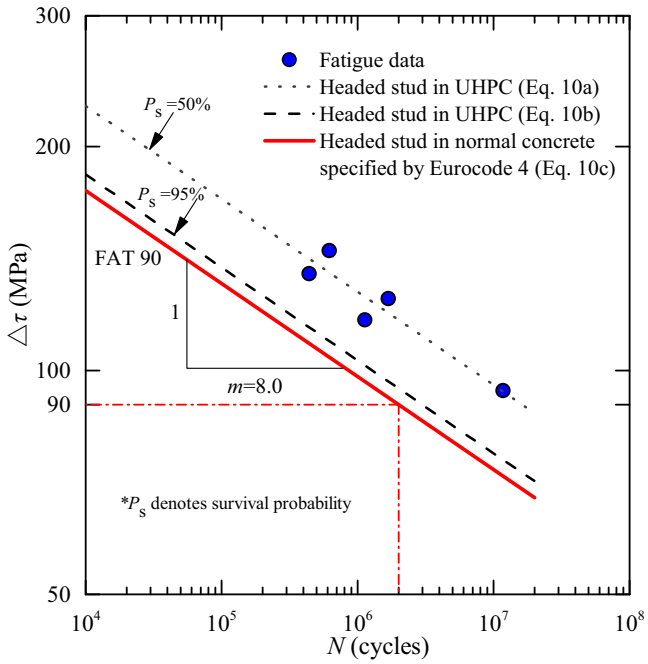

Fig. 12. *S-N* curves for headed studs against shear stress

than in normal concrete. Thus, both Eqs. (10*b*) and (10*c*) can be used in fatigue design of headed studs embedded in UHPC.

Dynamic Slip at Steel–UHPC Interface

As mentioned previously, the dynamic slip at the steel–UHPC interface was recorded at a sampling frequency of 100 Hz. Considering that the slip increases very slowly throughout the fatigue test, and that saving all data would require a substantial amount of memory, the dynamic slip was recorded intermittently during the fatigue tests.

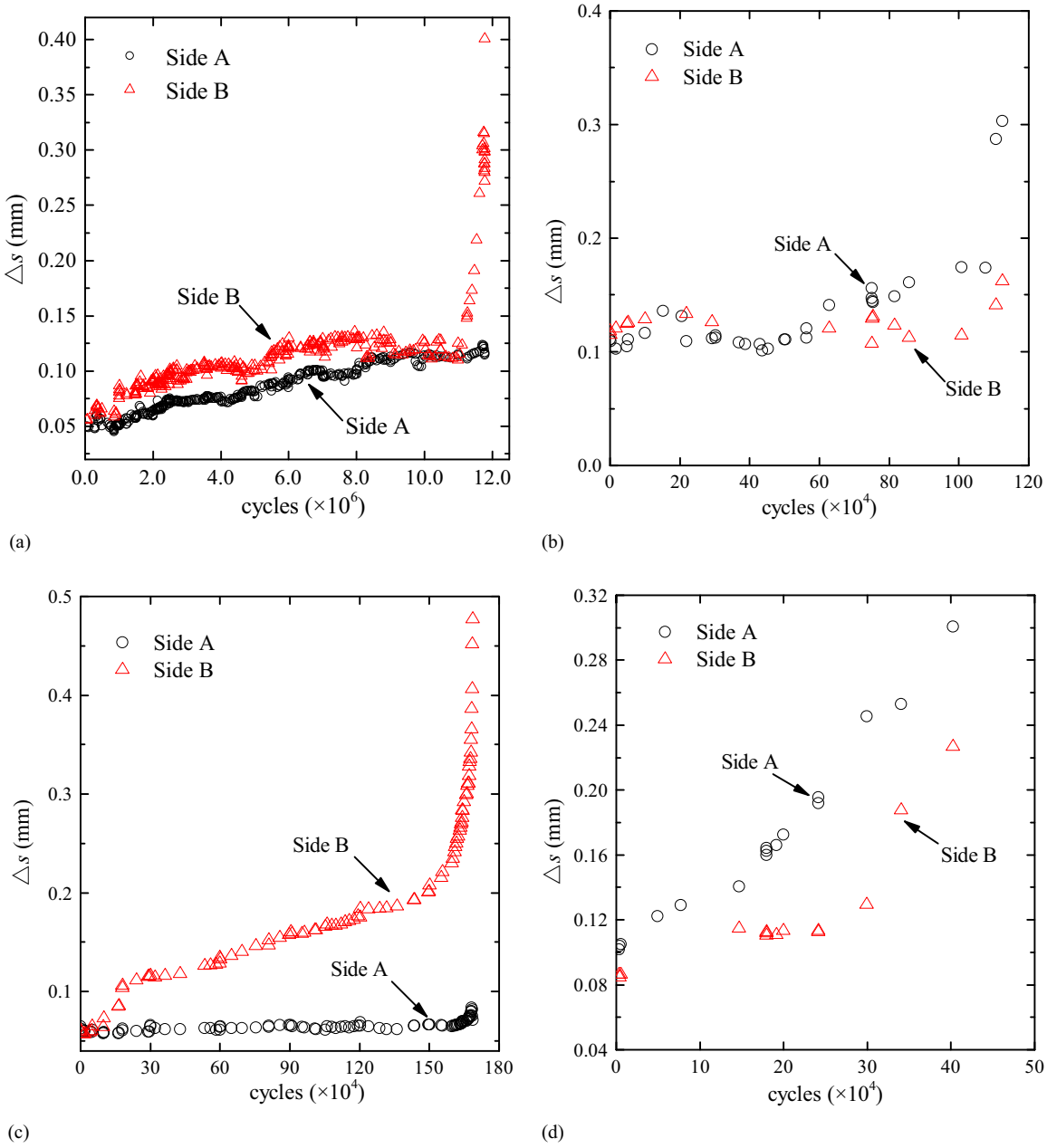

Fig. 13. Dynamic relative slips at steel–UHPC interface: (a) Specimen FAT-1; (b) Specimen FAT-2; (c) Specimen FAT-3; (d) Specimen FAT-4

It was found that, during the fatigue tests, the peak slips (i.e., s_{max} or s_{min}) were very sensitive to the anchorage condition of the test setup. Because each fatigue test lasted for days or even months (e.g., FAT-1), the anchorage between the steel plates and the ground gradually became loose during the fatigue test and was tightened from time to time, as did the anchorage of the actuator. In addition, the fatigue test was halted after a certain number of cycles for performing the static test. All of these factors caused interruptions to a continuing testing condition. As a consequence, the peak slips did not exhibit a smooth trend throughout the fatigue test. Fortunately, the relative slips (i.e., $\Delta s = s_{max} - s_{min}$) exhibited a smooth trend. Thus, relative slips instead of peak slips are analyzed and discussed here, as shown in Fig. 13.

According to Fig. 13, the relative dynamic slips generally increase with the loading cycles. Most of the time during the fatigue test, the slips increased approximately linearly with the number of loading cycles. However, prior to failure, there was a sudden increase of the slips, and such increase was especially noticeable on the side where the failure occurred.

Based on the dynamic slips obtained, the slip rates can be calculated for all of the specimens. Prior to calculating the slip rates, relevant references on calculating the slip rate of headed studs in normal concrete are reviewed here.

Hallam (1976) proposed an equation to calculate the slip rate based on the fatigue test on push-out specimens [Eq. (11)]. The shear force range is the key factor that affects the slip rate. Valente (2007) proposed a similar equation for headed studs in lightweight concrete, as shown in Eq. (12)

$$\log \delta = -10 + 12.99 \frac{\Delta F}{Q_u} \tag{11}$$

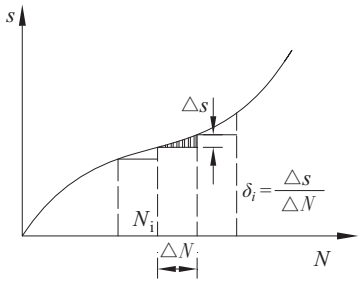

Fig. 14. Calculation of slip rate

Table 6. Calculated Slip Rates

Specimen	ΔF (kN)	$\Delta F/Q_u$	log δ	δ (mm/cycle)
FAT-1	100	0.21	–7.6425	2.278×10^{-8}
FAT-2	124	0.26	–7.0101	9.771×10^{-8}
FAT-3	133	0.28	–6.6064	2.475×10^{-7}
FAT-4	143	0.30	–6.4213	3.791×10^{-7}

$$\log \delta = -7.11 + 5.79 \frac{\Delta F}{Q_u} \tag{12}$$

where δ = slip rate of headed stud (mm/cycle); ΔF = shear force range per headed stud (kN); and Q_u = shear strength of a headed stud (kN).

Oehlers and Coughlan (1986) also proposed an equation for predicting the slip rate, as shown in Eq. (13). In this equation, the slip rate is governed by both the force range and the diameter of the headed stud

$$\delta = 1.70 \times 10^{-5} \frac{\Delta F}{Q_u} d \tag{13}$$

where δ = slip rate of headed stud (mm/cycle); ΔF = shear force range per headed stud (kN); Q_u = shear strength of a headed stud; and d = diameter of headed studs (mm).

The calculation of the slip rate for the headed studs in UHPC is composed of three steps. First, the dynamic slips on the two steel–UHPC interfaces were averaged for each case. Second, the fatigue life (N) for each specimen was divided into many segments, and the slip rate within each segment was calculated as $\delta_i = \Delta s/\Delta N$. Considering the value of δ_i is very small, $\log \delta_i$ was calculated. Finally, all of the $\log \delta_i$ values were averaged to calculate the average slip rate ($\log \delta$) for each specimen. The calculating process can be explained using Fig. 14. The calculated results are shown in Table 6. In the table, the values of $\triangle F/Q_u$ were calculated for a single-headed stud.

The calculated slip rates were compared to those of headed studs in normal concrete. Considering that no fatigue tests were performed for headed studs in normal concrete in this study, Eqs. (11)–(13) were used to calculate the slip rates. The comparisons are shown in Fig. 15.

As can be seen in Fig. 15, the higher the force range is, the higher the slip rate is. In addition, the figure demonstrates that the slip rate of the headed studs in UHPC is lower than that of the headed studs in normal concrete, which is likely attributed to the high strength of UHPC.

In addition, a linear fitting was performed for the slip-rate data presented in Table 6, and it was found that the relationship between the slip rate and the force range can be expressed by Eq. (14)

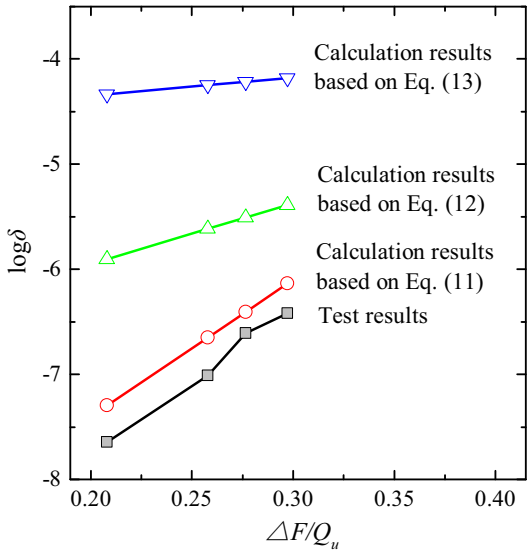

Fig. 15. Comparison of slip rates

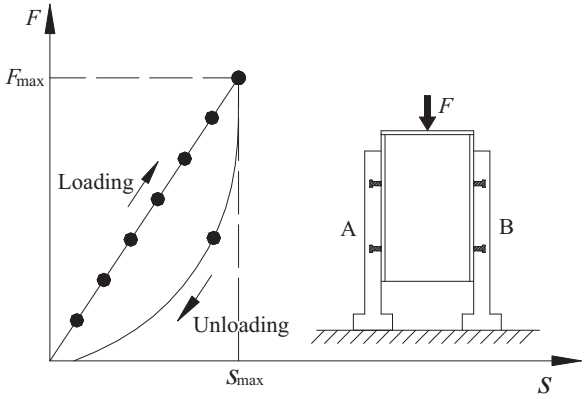

Fig. 16. Static tests performed during fatigue tests

$$\log \delta = -10.574 + 14.053 \frac{\Delta F}{Q_u} \tag{14}$$

Static Slip at Steel–UHPC Interface

During the fatigue test, static tests were performed when the fatigue loading reached certain numbers of cycles, aiming to record the degradation of the shear stiffness of the headed studs. The target maximum load in the static tests was equal to the maximum fatigue load (F_{max}), as shown in Table 4. Consequently, the static tests in this subsection are different from the aforementioned pure static tests in that the maximum load applied here is quite lower than the shear strength. The reason is that, if a static load significantly greater than F_{max} was applied, the specimens may fail in the static tests because the fatigue damage gradually accumulated in the headed studs in the previous fatigue test.

The static load was increased monotonically, and the load increments were slightly different between different specimens. Each static test was divided into six to seven load steps. When the load reached the maximum value, the specimen was then unloaded. The unloading process consisted of two steps. In the first step, the load was decreased to approximately half of the

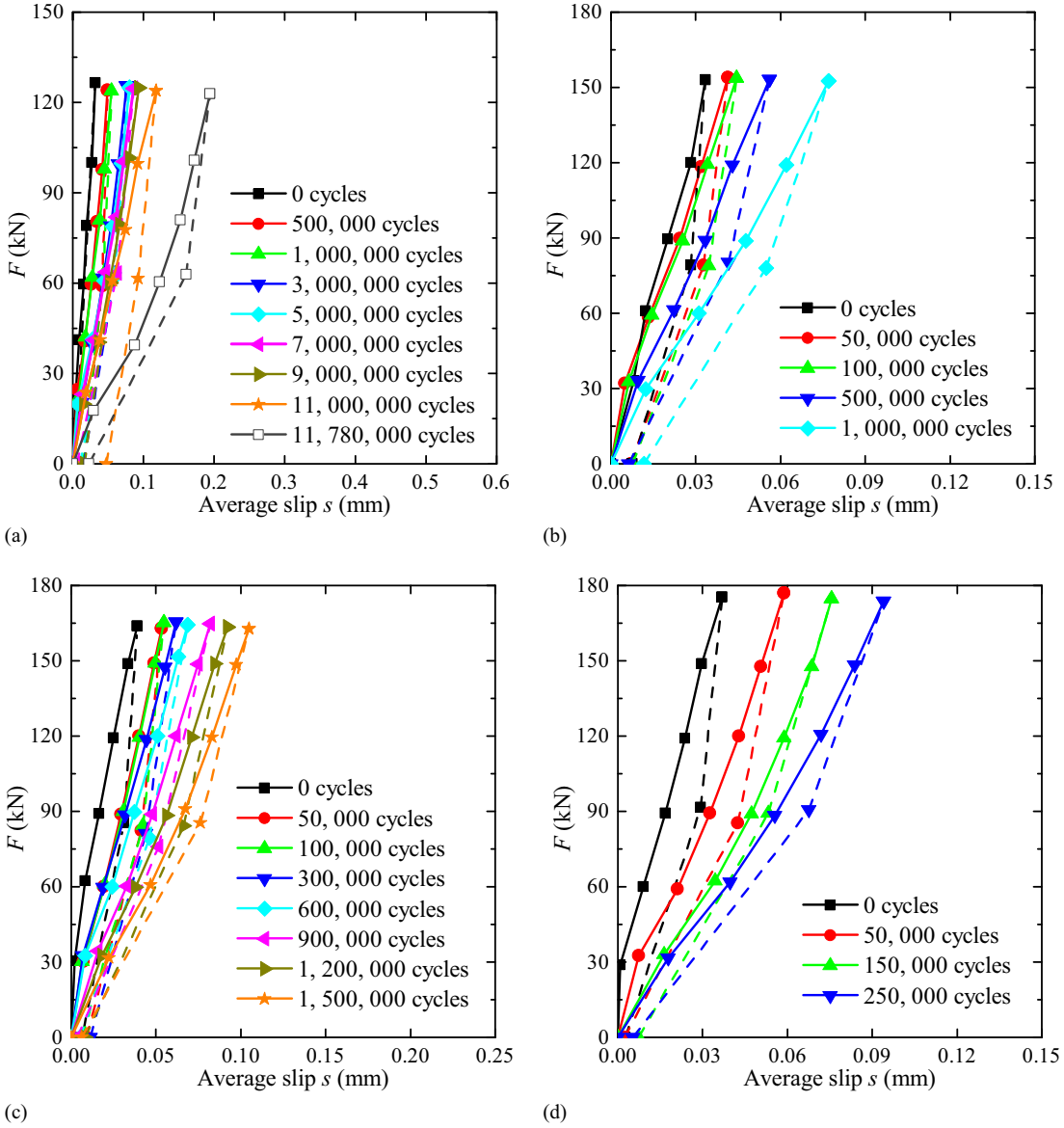

Fig. 17. Static load-slip curves obtained during fatigue tests: (a) Specimen FAT-1; (b) Specimen FAT-2; (c) Specimen FAT-3; (d) Specimen FAT-4

maximum load, whereas in the second step, the load was thoroughly removed. Fig. 16 shows a schematic drawing of the loading and unloading processes.

The load-slip curves obtained in the static tests are plotted in Fig. 17. Because of unavoidable eccentricity of both the loading and the anchoring systems, the slips on the two sides of each specimen were unequal. Thus, the average slips from Sides A and B were obtained, as presented in Fig. 17. In the figure, the solid lines represent the loading process, whereas the dashed lines represent the unloading process.

Fig. 17 implies that the load-slip curve during each static test is approximately linear, possibly because the maximum load applied to the specimens was small relative to their static shear strengths. When the number of loading cycles increases, the slip at the interface increases under the same static load, indicating that the shear stiffness at the interface decreases.

To gain more insight into the change of shear stiffness of the headed studs with the fatigue damage accumulated, the shear stiffness of the headed studs was calculated using the results from each static test during the fatigue test according to the equation $k' = F_{max}/s_{max}$ (Fig. 16). The relationship between the relative shear stiffness and the number of loading cycles is depicted in Fig. 18. The relative shear stiffness here refers to the ratio between the current shear stiffness of the headed stud after experiencing a certain number of fatigue loading cycles and its initial shear stiffness prior to being tested. It should be noted that, in Fig. 18, the abscissa refers to relative number of loading cycles (N/N_f).

Fig. 18 clearly shows that the shear stiffness of the headed studs decreases with increasing loading cycles. A sharp decrease can be observed at the early stage of the endurance, which is followed by an approximately linear decrease. In addition, for FAT-1, there was another sharp decrease prior to the fatigue failure. The first sharp decrease was likely due to the initiation and development of slip cracks at the steel–UHPC interface. In FAT-1, slip cracks were first observed when the number of loading cycles reached 2.1 million cycles (i.e., $N/N_f = 0.18$), as shown in Fig. 19(a). The second sharp decrease was probably related to the fatigue load–induced plastic deformation at the root of headed studs prior to the failure ($N/N_f =$

0.97), which caused a sudden debonding at the steel–UHPC interface [Fig. 19(b)].

To correlate the relative shear stiffness to the relative fatigue life, a nonlinear fitting was performed on the data in Fig. 18. Hanswille et al. (2007b) reported fatigue test results for the conventional headed studs in normal concrete, and proposed a function to correlate the slip to the loading cycle. By comparing the shape of the curves in Fig. 18 to the curves presented in the reference, it can be seen that the two figures have a similar shape. Thus, a function similar to that used by Hanswille et al. (2007b) was used here and is shown in Eq. (15), whereas the fitted results are shown in Table 7. For comparison, the fitted results are plotted against the test results for each specimen, as shown in Fig. 20

$$\eta = \begin{cases} 1 & N = 0 \\ C_1 + C_2 \mathrm{In}\left(\dfrac{1}{N/N_\mathrm{f}} - 1\right) & 0 < N < N_\mathrm{f} \end{cases} \tag{15}$$

where η = relative shear stiffness; and C_1 C_2 = fitted coefficients.

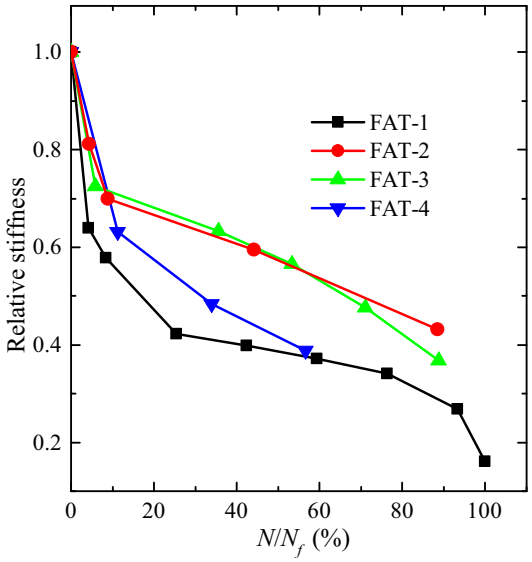

Fig. 18. Relative shear stiffness against relative loading cycles

According to Fig. 20, the fitted curves correlate well with the test results, indicating that the fitted curves can adequately reflect the three phases of the shear stiffness–reduction trend. In addition, the figure also shows that, when the fatigue cycle is 50% of the endurance life, the shear stiffness reduction can be as high as 40–60%.

Summary and Conclusions

This paper reveals the basic behavior of short-headed studs embedded in UHPC through static and fatigue load tests on push-out specimens. Based on the results from the present study, the following conclusions can be drawn:

1. The pure static load tests on the specimens showed that the failure of the specimens was caused by the fracture of the headed studs from the root, whereas the UHPC layer was still in good condition except for small localized damage around the headed studs at the inner surface. Thus, although the headed studs had a low height-to-diameter ratio of 2.7, they can develop full strength in thin UHPC layers.
2. The shear stiffness of the short-headed studs was obtained by applying the secant slope method to the load-slip curves obtained in the static tests. It was found that the headed studs had a shear stiffness of k = 266–396 kN/mm per stud based on different calculation methods.
3. Based on the fatigue test data, a design *S-N* curve with 95% survival probability was proposed for the headed studs embedded in UHPC. The proposed *S-N* curve lies slightly above the *S-N* curve specified in Eurocode 4 for headed studs in normal concrete.
4. The dynamic slips as well as the static load–induced slips were observed at the steel–UHPC interface during the fatigue tests. Both types of slips increased continuously with the increasing loading cycles, and a sudden increase in slips was observed prior to failure. The static load–induced shear stiffness of the headed studs was found to decrease with the loading cycles.

Table 7. Nonlinear Fitting Results of Shear Stiffness Reduction Function

Specimen	F_{max}/Q_u	F_{min}/Q_u	$\Delta F/Q_u$	C_1	C_2
FAT-1	0.25	0.05	0.21	0.4291	0.0475
FAT-2	0.31	0.06	0.26	0.5803	0.0496
FAT-3	0.34	0.06	0.28	0.5449	0.0528
FAT-4	0.36	0.06	0.30	0.4461	0.0617

N/N_f=0.18 N/N_f=0.97

Fig. 19. Slip cracks observed at Side B of Specimen FAT-1

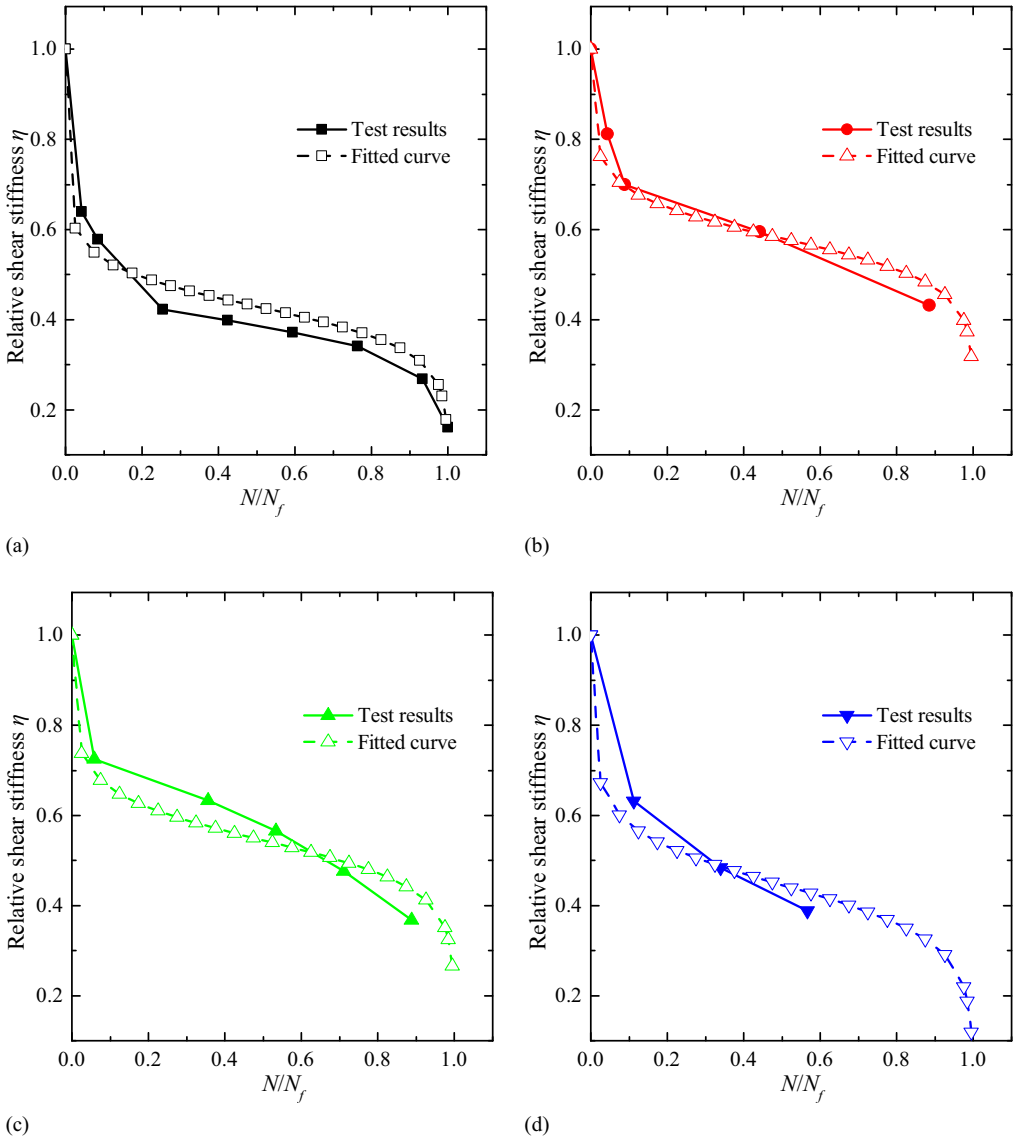

Fig. 20. Comparison between fitted curve and tested results: (a) Specimen FAT-1; (b) Specimen FAT-2; (c) Specimen FAT-3; (d) Specimen FAT-4

Acknowledgments

The authors thank the following funders for their support: the National Natural Science Foundation of China (Grant 51178177), the Transportation Science and Technology Major Project sponsored by the Ministry of Transport of China (Grants 2011318494160 and 2013318798320), the Transport Agency of Zhejiang Province of China (Grant 2015J24), and the Scientific Research Innovation Program for Postgraduate Studies in the Hunan Province of China (Grant CX2011B150).

References

AASHTO. (2012). *AASHTO LRFD bridge design specifications*, Washington, DC.

An, L., and Cederwall, K. (1996). "Push-out tests on studs in high strength and normal strength concrete." *J. Constr. Steel Res.*, 36(1), 15–29.

Buitelaar, P., Braam, R., and Kaptijn, N. (2004). "Reinforced high performance concrete overlay system for rehabilitation and strengthening of orthotropic steel bridge decks." *Proc., 1st Int. Orthotropic Bridge Conf.*, ASCE, Sacramento, CA, Aug. 25–27, 384–401.

Civjan, S. A., and Singh, P. (2003). "Behavior of shear studs subjected to fully reversed cyclic loading." *J. Struct. Eng.*, 10.1061/(ASCE)0733-9445(2003)129:11(1466), 1466–1474.

Dieng, L., Marchand, P., Gomes, F., Tessier, C., and Toutlemonde, F. (2013). "Use of UHPFRC overlay to reduce stresses in orthotropic steel decks." *J. Constr. Steel Res.*, 89, 30–41.

Doinghaus, P., Goralski, C., and Will, N. (2003). "Design rules for composite structures with high performance steel and high performance concrete." *Proc., Conf. on High Performance Materials in Bridges*, ASCE, Reston, VA, 139–149.

ECS (European Committee for Standardization). (2005). *Eurocode 4: Design of composite steel and concrete structures, part 1-1: General rues and rules for buildings (EN 1994-1-1)*, Brussels, Belgium.

GAQSIQOC (General Administration of Quality Supervision). (2002). *Cheese head studs for arc stud welding (GB/T 10433-2002)*, Inspection and Quarantine of China, Beijing, China, 1–2 (in Chinese).

Graybeal, B. A. (2005). "Characterization of the behavior of ultra-high performance concrete." Ph.D. thesis, Univ. of Maryland, College Park, MD.

Hajar, Z., Novarin, M., Servant, C., Généreux, G., Przybyla, D., and Bitar, D. (2013). "Innovative solution for strengthening orthotropic decks using UHPFRC: The Illzach Bridge." *Proc., RILEM-fib-AFGC Int. Symp. on Ultra-High Performance Fibre-Reinforced Concrete*, RILEM, Paris, 117–126.

Hallam, M. W. (1976). "The behavior of stud shear connectors under repeated loading." *Research Rep. No. R281*, School of Civil Engineering, Univ. of Sydney, Sydney, Australia.

Hanswille, G., Porsch, M., and Ustundag, C. (2007a). "Resistance of headed studs subjected to fatigue loading: Part I: Experimental study." *J. Constr. Steel Res.*, 63, 475–484.

Hanswille, G., Porsch, M., and Ustundag, C. (2007b). "Resistance of headed studs subjected to fatigue loading. Part II: Analytical study." *J. Constr. Steel Res.*, 63, 485–493.

Hegger, J., Sedlacek, G., Döinghaus, P., Trumpf, H., and Eligehausen, R. (2001). "Studies on the ductility of shear connectors when using high-strength steel and high-strength concrete." *Proc., Int. Symp. on Connections between Steel and Concrete*, RILEM Publications SARL, Cedex, France, 1025–1045.

Hobbacher, A. F. (2007). *Recommendations for fatigue design of welded joints and components (XIII-2151-07/XV-1254-07)*, International Institute of Welding, Paris.

Johnson, R., and May, I. (1975). "Partial-interaction design of composite beams." *Struct. Eng.*, 8(53), 305–311.

JSSC (Japan Society of Civil Engineers). (2002). *Guidelines for performance-based design of steel-concrete hybrid structures*, Tokyo.

Kang, J. Y., Park, J. S., Jung, W. T., and Keum, M. S. (2014). "Evaluation of the shear strength of perfobond rib connectors in ultra high performance concrete." *Eng.*, 6(13), 989–999.

Kim, J. S., Kwark, J., Joh, C., Yoo, S. W., and Lee, K. C. (2015). "Headed stud shear connector for thin ultrahigh-performance concrete bridge deck." *J. Constr. Steel Res.*, 108, 23–30.

Li, J., Yang, B., Shao, X. D., and Li, J. (2016). "Research on shear fatigue of studs for composite deck system with steel slab and thin CRRPC layer." *China Civ. Eng. J.*, 49(6), 67–75 (in Chinese).

Luo, Y., Hoki, K., Hayashi, K., and Nakashima, M. (2015a). "Behavior and strength of headed stud-SFRCC shear connection. I: Experimental study." *J. Struct. Eng.*, 10.1061/(ASCE)ST.1943-541X.0001363, 04015112.

Luo, Y., Hoki, K., Hayashi, K., and Nakashima, M. (2015b). "Behavior and strength of headed stud-SFRCC shear connection. II: Strength evaluation." *J. Struct. Eng.*, 10.1061/(ASCE)ST.1943-541X.0001372, 04015113.

Mainston, R. J., and Menzies, J. B. (1967). "Shear connectors in steel-concrete composite beams for bridges. Part I: Static and fatigue tests on push-out specimens." *Concrete*, 1(9), 291–302.

MHURDOC (Ministry of Housing and Urban-Rural Development of China). (2013). *Code for design of steel and concrete composite bridges (GB 50917-2013)*, China Planning Press, Beijing (in Chinese).

Murakoshi, J., Yanadori, N., and Ishii, H. (2007). "Research on steel fiber reinforced concrete pavement for orthotropic steel deck as a countermeasure for fatigue." *Proc., 23th U.S.-Japan Bridge Engineering Workshop, Tsukuba, Japan*, Public Works Research Institute of Japan, Ibaraki-ken, Japan.

Nie, J. G., and Shen, J. M. (1994). "A general formula for predicting the deflection of simply supported composite steel-concrete beams with the consideration of slip effect." *Eng. Mech.*, 11(1), 21–27 (in Chinese).

Oehlers, D. J., and Coughlan, C. G. (1986). "The shear stiffness of stud shear connections in composite beams." *J. Constr. Steel Res.*, 6(4), 273–284.

Ollgaard, J. G., Slutter, R. G., and Fisher, J. W. (1971). "Shear strength of stud connectors in lightweight and normal-weight concrete." *AISC Eng. J.*, 8(2), 55–64.

Rauscher, S., and Hegger, J. (2008). "Modern composite structures made of high performance materials." *Proc., Composite Construction in Steel and Concrete Conf. VI*, Devil's Thumb Ranch, Tabernash, CO, ASCE, Reston, VA.

Shao, X. D., Yi, D. T., Huang, Z. Y., Zhao, H., Chen, B., and Liu, M. L. (2013). "Basic performance of the composite deck system composed of orthotropic steel deck and ultrathin RPC layer." *J. Bridge Eng.*, 10.1061/(ASCE)BE.1943-5592.0000348, 417–428.

Shariati, A., Ramlisulong, N., and Shariati, M. (2012). "Various types of shear connectors in composite structures: A review." *Int. J. Phys. Sci.*, 7(22), 2876–2890.

Slutter, R. G., and Driscoll, G. C. (1961). "Research on composite design at Lehigh University." *Proc., 13th National Engineering Conf. of AISC*, AISC Press, Minneapolis.

Slutter, R. G., and Fisher, J. W. (1966). "Fatigue strength of shear connectors." *Highway Res. Rec.*, 147, 65–88.

Valente, M. I. (2007). "Experimental studies on shear connection systems in steel and lightweight concrete composite bridges." Ph.D. thesis, Univ. of Minho, Braga, Portugal.

Wang, Y. (1998). "Deflection of steel-concrete composite beams with partial shear interaction." *J. Struct. Eng.*, 10.1061/(ASCE)0733-9445(1998)124:10(1159), 1159–1165.

Xue, W. C., Ding, M., Wang, H., and Luo, Z. (2008). "Static behavior and theoretical model of stud shear connectors." *J. Bridge Eng.*, 10.1061/(ASCE)1084-0702(2008)13:6(623), 623–634.